Research Square

Preprints are preliminary reports that have not undergone peer review.
They should not be considered conclusive, used to inform clinical practice,
or referenced by the media as validated information.

Differential Roles of VEGFA and FGF2 in Vascular Maturation and Regression of Laser-Induced Choroidal Neovascularization

Yuichi Yamamoto
yamamoto.yui@kmu.ac.jp
Kansai Medical University
Haruhiko Yamada
Kansai Medical University
Hidetsugu Mori
Kansai Medical University
Yuki Hattori
Kansai Medical University
Kaito Yokota
Niimi Eye Clinic
Masatoshi Omi
Kansai Medical University
Megumi Kitamura
Kansai Medical University
Masayuki Ohnaka
Kansai Medical University
Hisanori Imai
Kansai Medical University

Article

Keywords: VEGF, FGF2, OCTA, Ang1/Ang2, Apelin, TSP1

Posted Date: May 19th, 2026

DOI: https://doi.org/10.21203/rs.3.rs-9521362/v1

License: This work is licensed under a Creative Commons Attribution 4.0 International License.
Read Full License

Additional Declarations: No competing interests reported.

Abstract

Angiogenesis is regulated by a dynamic balance between proangiogenic and antiangiogenic factors. VEGFA and FGF2 are both major proangiogenic factors, but have different modes of action. To explore the role of VEGFA and FGF2 in retinal diseases, we induced choroidal neovascularization by laser photocoagulation (Li-CNV) in wild-type (WT) mice and mice transgenic for VEGF (rho/VEGF-tg), FGF2 (rho/FGF2-tg) or FGF2/VEGF (rho/FGF2/VEGF-tg). We then evaluated CNV dynamics longitudinally using optical coherence tomography angiography (OCTA) and cross-sectionally using choroidal flat mounts of eyes from the treated mice. We also analyzed mRNA expression levels of vascular maturation factors (PDGFRβ, Ang1/Ang2, apelin) and antiangiogenic factors (TSP1, PEDF) by RT-qPCR. The area of Li-CNV lesions peaked on day 7 post-photocoagulation and regressed thereafter. Rho/FGF2-tg mice and rho/FGF2/VEGF-tg mice showed increased CNV area on day 7 compared to WT mice, whereas rho/VEGF-tg mice and rho/FGF2/VEGF-tg mice showed persistent CNV on day 28 compared to WT mice. RT-qPCR of rho/FGF2-tg mice showed elevated PDGFRβ, Ang1, apelin and TSP1 levels during the proliferative phase, and persistent TSP1 upregulation after CNV regression. Meanwhile, rho/VEGF-tg mice had reduced PEDF levels during the regression phase. These findings support that VEGFA and FGF2 differentially regulate CNV dynamics, including formation, maturation, and regression.

Introduction

Angiogenesis is regulated by a dynamic balance between proangiogenic and antiangiogenic factors. Angiogenesis driven by proangiogenic factors, including vascular endothelial growth factor (VEGF), platelet-derived growth factor (PDGF), fibroblast growth factors (FGFs), transforming growth factor-β (TGFβ), and angiopoietins (Ang), is antagonized by endogenous antiangiogenic factors, including thrombospondin-1 (TSP1), pigment epithelium-derived factor (PEDF), and endostatin [1, 2]. The balance between these opposing factors controls the direction of angiogenesis toward activation, stabilization, or regression.

Among these factors, VEGF is the most important for the process of angiogenesis. VEGF is considered to play a central role in pathological angiogenesis and has been extensively investigated as a therapeutic target in oncology, the circulatory system, and ophthalmology. During the sprouting phase of angiogenesis, VEGF stimulated by HIF1 forms concentration gradients composed of its soluble and matrix-bound isoforms that induce the expression of Delta-like ligand 4 (DLL4) and in turn promotes endothelial cell migration [1, 3]. VEGF also suppresses endothelial cell apoptosis by activating the PI3K/Akt pathway via the Flk-1/KDR (VEGFR2) receptor, and functions as a critical survival factor for existing vessels [4, 5]. In contrast, antiangiogenic factors, including TSP1 and PEDF, counteract VEGF signaling, promote endothelial apoptosis, and contribute to vascular regression [6, 7].

Clinically, anti-VEGF agents have become the mainstay for treating retinal vascular diseases such as neovascular age-related macular degeneration (nAMD), branch retinal vein occlusion (BRVO), and diabetic macular edema (DME). Although therapeutic options for these diseases have dramatically

improved and offer good visual outcomes, patients must receive repeated intravitreal injections of anti-neovascular agents such as anti-VEGF drugs to maintain treatment efficacy. Moreover, a subset of patients have suboptimal responses or are resistant to treatment [8, 9]. Thus, a better understanding of the mechanisms of the angiogenic regulatory network that governs vascular maturation, stabilization, and regression is needed to discover additional therapeutic targets beyond anti-VEGF.

The proangiogenic factor FGF2 is a multifunctional growth factor that promotes endothelial cell proliferation and also interactively regulates vascular maturation. FGF2 induces VEGF expression and upregulates PDGF, Ang1, and vascular endothelial cadherin (VE-cadherin) in pericytes that promotes their recruitment and participation in tight junction formation, and vessel stabilization [10]. Capillaries formed in response to FGF2 tend to be less permeable and morphologically different from those induced predominantly by VEGF [11]. Furthermore, FGF2 promotes angiogenesis through VEGF-independent pathways, including the apelin–APJ axis, which enhances endothelial proliferation via Akt/mTOR signaling [12–14]. In parallel with anti-VEGF strategies, FGF signaling recently has attracted attention as a therapeutic target for nAMD, and large-scale clinical trials of anti-FGF agents are ongoing [15, 16].

In animal models, both VEGF and FGF2 can induce and augment choroidal neovascularization (CNV) [17, 18]. Wong et al. also demonstrated that combined administration of VEGF and FGF2 induces CNV formation [19], but VEGF and FGF2 administered individually have no effect on angiogenesis. These previous studies evaluated each factor alone or in combination, but did not directly examine how VEGF and FGF2 contribute to CNV within the same in vivo experimental system.

In this study, we used transgenic mice expressing VEGF in the outer retina (rho/VEGF transgenic mice; rho/VEGF-tg mice) [20] or FGF2 in photoreceptors (rho/FGF2 transgenic mice; rho/FGF2-tg mice) [21] under the control of the rhodopsin promoter. These transgenes drive local production of proangiogenic factors endogenously within the retina, and allow evaluation of the effects of VEGF and FGF2 on CNV without the iatrogenic insult associated with intravitreal injections.

We aimed to further clarify the respective contributions of VEGF and FGF2 to pathological choroidal neovascularization and explore the potential of novel treatment strategies that target vascular growth, stability, and regression. Here we induced choroidal neovascularization by laser photocoagulation (Li-CNV) in wild-type (WT), rho/VEGF-tg, and rho/FGF2-tg mice, as well as rho/FGF2/VEGF double transgenic (rho/FGF2/VEGF-tg) mice. Using mouse optical coherence tomography angiography (OCTA) and choroidal flat mounts, we longitudinally evaluated VEGFA- and FGF2-driven vascular changes. We also used real-time quantitative PCR (RT-qPCR) to analyze the mRNA expression levels of different vascular maturation factors like PDGFR and Ang1/Ang2, as well as antiangiogenic factors related to vascular regression, including TSP1 and PEDF. By integrating these structural and molecular readouts, we sought to delineate the distinct roles of VEGF and FGF2 in vascular maturation, stabilization, and regression associated with CNV. To our knowledge, this is the first in vivo study to directly compare VEGF- and FGF2-driven Li-CNV in a double transgenic line, under identical conditions, and to combine longitudinal OCTA imaging with molecular profiling of vascular maturation and regression markers.

Results

1. Immunolabeled cryosections

We first confirmed the expression and localization of human VEGFA and human FGF2 in WT, rho/VEGF-tg, rho/FGF2-tg, and rho/FGF2/VEGF-tg mice (Fig. 1). In WT mice, no specific immunoreactivity was observed with anti-human FGF2 or anti-human VEGFA antibodies. In rho/VEGF-tg mice, human VEGFA was locally present in the outer retina at sites corresponding to retinal neovascularization (arrowheads). No immunoreactivity was detected with the anti-human FGF2 antibody. In rho/FGF2-tg mice, human FGF2 was mainly localized to the outer nuclear layer (arrows). No immunoreactivity was detected with the anti-human VEGFA antibody. In rho/FGF2/VEGF-tg mice, human VEGFA was locally present in the outer retina at sites corresponding to retinal neovascularization (arrowheads) and human FGF2 was mainly localized to the outer nuclear layer (arrows).

2. Immunolabeled choroidal flat mounts

In all genotypes, CD31-positive cells were detected from day 3 post-photocoagulation (PC), and these cells were surrounded by PDGFR-positive and α-SMA-positive cells. At day 7 post-PC, CD31-positive neovascular endothelial cells with PDGFR-positive and α-SMA-positive mural cells were clearly detected (Fig. 2A). At days 14 and 21 post-PC, CD31-, PDGFR-, and α-SMA–positive cells associated with neovessels were detected. At day 28 post-PC, CD31- and PDGFR-positive neovascular cells were observed for all genotypes, whereas α-SMA–positive cells were absent in some eyes from WT and rho/FGF2-tg mice (Fig. 2B).

We quantified the area of CD31-positive CNV lesions on choroidal flat mounts (Fig. 2C). In all genotypes, Li-CNV lesions had the largest area at day 7 post-PC and the area decreased thereafter. At day 7 post-PC, the CD31-positive CNV area in rho/FGF2-tg mice was significantly larger than that in WT and rho/VEGF-tg mice ($p = 0.0072$ and $p = 0.0189$, respectively; Fig. 2A). Similarly, at day 7 post-PC, the CD31-positive CNV area in double transgenic rho/FGF2/VEGF-tg mice was significantly larger than that in WT and rho/VEGF-tg mice ($p = 0.0010$ and $p = 0.0014$, respectively; Fig. 2A).

By day 28 post-PC, the CNV areas had markedly regressed in all genotypes. However, in rho/VEGF-tg mice, the CNV area remained significantly larger than that in WT and rho/FGF2-tg mice ($p = 0.0237$ and $p = 0.0189$, respectively; Fig. 2B). In rho/FGF2/VEGF-tg mice, the area of CNV lesions regressed substantially, similar to that seen in rho/FGF2-tg mice, but the CD31-positive CNV area at day 28 remained significantly larger than that in WT and rho/FGF2-tg mice (both $p = 0.0010$; Fig. 2B).

3. OCTA imaging

In all genotypes, CNV lesions reached maximum size on day 7 post-PC. In WT and rho/FGF2-tg mice, Li-CNV lesions almost completely regressed by day 28 post-PC. In rho/VEGF-tg and rho/FGF2/VEGF-tg mice, CNV lesions did decrease in size after day 7, but residual lesions remained clearly visible at day 28 post-PC (Fig. 3A).

We defined the CNV area at day 7 post-PC as 100%, and then evaluated the residual CNV area at day 28 post-PC as a percentage. The vascular regression rate was calculated using the formula (CNV area on day 7-CNV area on day 28)/ CNV area on day 7 x 100 (WT: 49%; rho/VEGF-tg: 16%; rho/FGF2-tg: 56%; rho/FGF2/VEGF-tg: 33%). The vascular regression rate in rho/VEGF-tg mice was significantly lower than that for WT and rho/FGF2-tg mice ($p = 0.0092$ and $p = 0.0019$, respectively; Fig. 3B). Meanwhile, for rho/FGF2/VEGF-tg mice the vascular regression rate did not significantly differ from that for rho/VEGF-tg and rho/FGF2-tg mice ($p = 0.2621$ and $p = 0.0844$, respectively; Fig. 3B).

4. RT-qPCR (Fig. 4A-H)

First, we confirmed the transgene expression levels. Across all conditions, the VEGFA mRNA expression level was significantly higher in rho/VEGF-tg and rho/FGF2/VEGF-tg mice than in WT and rho/FGF2-tg mice, and the FGF2 mRNA expression level was significantly higher in rho/FGF2-tg and rho/FGF2/VEGF-tg mice relative to WT and rho/VEGF-tg mice (all $p < 0.05$). These results confirmed the robust expression of each transgene in the corresponding transgenic lines.

Non-PC

For animals without PC, Ang1 and TSP1 mRNA expression levels in rho/FGF2/VEGF-tg mice were significantly higher than those in WT mice ($p = 0.0050$ and $p = 0.0039$, respectively).

Day 7 post-PC

At day 7 post-PC, PDGFRβ, Ang1, apelin, and TSP1 mRNA expression levels in rho/FGF2-tg mice were significantly higher than those in WT mice ($p = 0.0055$, $p = 0.0055$, $p < 0.0001$, and $p = 0.0006$, respectively).

In rho/VEGF-tg mice, the Ang2 mRNA expression level was significantly higher than that in WT mice ($p = 0.0031$). In rho/FGF2/VEGF-tg mice, PDGFRβ, Ang2, and apelin mRNA expression levels were significantly higher than those in WT mice ($p = 0.0046$, $p = 0.0280$, and $p = 0.0015$, respectively). Moreover, Ang1 and TSP1 mRNA expression levels were not significantly higher than those in WT mice ($p = 0.4806$, and $p = 0.3267$, respectively).

Day 14 post-PC

At day 14 post-PC, Ang1 and TSP1 mRNA expression levels in rho/FGF2-tg mice remained significantly higher than those in WT mice ($p = 0.0010$ and $p = 0.0229$, respectively). The PEDF mRNA expression level in rho/VEGF-tg mice was significantly lower than that in WT mice ($p = 0.0055$).

In rho/FGF2/VEGF-tg mice, Ang1 and TSP1 mRNA expression levels were not significantly higher than those in WT mice ($p = 0.1324$, $p = 0.0170$, and $p = 0.0540$, respectively).

Day 28 post-PC

At day 28 post-PC, PDGFRβ mRNA expression levels in the rho/FGF2-tg and rho/FGF2/VEGF-tg mice were significantly higher than those in WT mice ($p = 0.0370$ and $p = 0.0492$, respectively). The TSP1 mRNA expression level was significantly higher in rho/FGF2-tg, rho/VEGF-tg, and rho/FGF2/VEGF-tg mice than in WT mice ($p = 0.0157$, $p = 0.0267$, and $p = 0.0001$, respectively). In addition, the apelin mRNA expression level at day 28 post-PC in rho/FGF2/VEGF-tg mice was significantly higher than that in WT mice ($p = 0.0070$).

Discussion

The Li-CNV model is an established experimental system for studying choroidal neovascularization associated with nAMD. According to a previous report [22], the course of Li-CNV can be divided into three phases: i) an initial inflammatory response that characterizes onset of a proliferative phase; ii) a proliferative phase during which neovascular complexes become apparent around day 3 after PC and reach maximum size around day 7; and iii) a regression phase in which CNV lesions shrink and partially regress. A major limitation in CNV research is the difficulty of sequentially evaluating temporal changes within the same eye. To address this limitation, we used OCTA to track CNV dynamics longitudinally in vivo. OCTA is a noninvasive method that allows repeated visualization of the retinal and choroidal vasculature and does not require dye injection or sacrifice of the animal.

Although VEGFA and FGF2 are both major proangiogenic factors, their modes of action in vascular biology differ. VEGFA promotes endothelial differentiation, migration, and proliferation, regulates inter-endothelial junctions, and suppresses endothelial cell apoptosis [3, 4]. FGF2 stimulates proliferation of both endothelial and mural cells and contributes to vascular maturation and stabilization [11, 23]. To our knowledge, this is the first study to make a direct comparison of CNV morphology and temporal behavior under conditions in which VEGFA or FGF2 was selectively overexpressed either alone or together within the same retinal microenvironment.

Moreover, we believe that this is the first study to directly compare laser-induced choroidal neovascularization (Li-CNV) induced by VEGFA and FGF2 under identical experimental conditions, including double transgenic mice expressing both human VEGFA and FGF2, using a combination of longitudinal OCTA imaging and molecular profiling for vascular maturation and regression markers. By combining OCTA, choroidal flat mount analysis, and RT-qPCR to evaluate WT, rho/VEGF-tg, rho/FGF2-tg, and rho/FGF2/VEGF-tg mice, we delineated the similarities and differences in the roles of VEGFA and FGF2 in CNV formation, maturation, and regression.

1. Different effects of VEGFA and FGF2 on CNV dynamics

We took advantage of two transgenic mouse lines: rho/VEGF-tg and rho/FGF2-tg mice. Rho/VEGF-tg mice locally express high levels of VEGFA in photoreceptors under control of the rhodopsin promoter. These mice develop pathological outer retinal neovascularization that mimics the retinal angiomatous proliferation (RAP) model [20, 24, 25]. Rho/FGF2-tg mice overexpress FGF2 in photoreceptors but have no spontaneous pathological retinal neovascularization or marked structural abnormalities [21]. In rho/FGF2-tg mice exposed to PC that damages photoreceptors, extracellularly-released FGF2 promotes formation of extremely large CNV lesions [26].

Flat mount based CNV analysis

Consistent with findings by Yamada et al. [26], the flat mount analysis conducted in this study demonstrated that rho/FGF2-tg mice developed markedly enlarged Li-CNV lesions during the proliferative phase. Here we also observed that Li-CNV in rho/FGF2-tg mice exhibited the morphological features of mature vessels as evidenced by Li-CNV that was surrounded by PDGFR-positive pericytes and α-SMA-positive mural cells. Despite this apparent maturation, CNV lesions in rho/FGF2-tg mice regressed rapidly and shrank to sizes comparable to those in WT mice by day 28 post-PC. These findings were consistent with those of Hattori et al. [27], who found that FGF2 could robustly promote CNV formation and vascular maturation, but could not sustain CNV over the long term.

In rho/VEGF-tg mice, Li-CNV during the proliferative phase was not larger than that in WT mice and was smaller than that in both rho/FGF2-tg and rho/FGF2/VEGF-tg mice. Moreover, mature CNV in rho/VEGF-tg mice during the regression phase persisted for a longer period than that in WT and rho/FGF2-tg mice. We hypothesized that a continuously high level of VEGFA would promote CNV formation and a large area of CNV. However, our results showed that VEGFA did not contribute to CNV growth, but did enhance CNV survival. This result is consistent with that of Greenberg et al., who reported that VEGF can not only promote endothelial growth, but can also act as a negative regulator of vascular maturation by suppressing PDGFRβ signaling in mural cells [28]. Our results suggest that, on the one hand, VEGFA overexpression enhances endothelial proliferation, but on the other, does not sufficiently promote pericyte recruitment and vessel stabilization. As a result, CNV in rho/VEGF-tg mice would remain limited. VEGFA also provides a strong survival signal to endothelial cells that may contribute to the prolonged existence of CNV. Indeed, Gerber et al. referred to a mechanism by which VEGFA suppresses endothelial apoptosis via the PI3K/Akt pathway [5]. In our study, sustained VEGFA expression likely provides potent survival signals to CNV endothelial cells that contribute to poor regression and longer-term persistence of CNV in rho/VEGF-tg mice compared to that in WT mice.

Rho/FGF2/VEGF-tg mice exhibited features of the mice that were transgenic for only FGF2 or VEGF. In rho/FGF2/VEGF-tg mice at day 7 post-PC, the area of CNV was enlarged to a similar extent as that in rho/FGF2-tg mice, and at day 28 post-PC, the CNV area persisted similarly to that seen for rho/VEGF-tg mice.

OCTA-based CNV analysis

OCTA-based regression analysis showed that the CNV regression rate in rho/VEGF-tg mice was slower than that in WT and rho/FGF2-tg mice. This finding is consistent with results for the flat mounts. Based on known VEGF properties, we initially expected that CNV in rho/FGF2/VEGF-tg mice would persist to similar degrees as for rho/VEGF-tg mice. However, the regression rate in rho/FGF2/VEGF-tg mice was intermediate between rho/FGF2-tg mice and rho/VEGF-tg mice and was not significantly different from either line. This finding suggests that, in terms of CNV regression, the effects of FGF2 and VEGFA expressed together would not exceed the effect of FGF2 and VEGFA expressed individually.

2. Role of FGF2 and VEGF in CNV vascular maturation pathways

To investigate the mechanisms of vascular maturation caused by different actions of FGF2 and VEGF, we used RT-qPCR to evaluate the mRNA expression levels of genes involved in vascular maturation, stabilization, and regression. We first confirmed by RT–qPCR that the transgenes were highly expressed in rho/VEGF-tg, rho/FGF2-tg, and rho/FGF2/VEGF-tg mice without treatment and in treated mice on days 7, 14, and 28 post-PC. Next, we investigated the mRNA expression levels of the well-known vascular maturation factors PDGFRβ, Ang1, and Ang2. In animals without PC, Ang1 mRNA expression levels in rho/FGF2/VEGF-tg mice were significantly higher than those in WT mice. This result may reflect a transcriptional response associated with retinal neovascularization that is normally observed in rho/VEGF-tg mice. During the proliferative phase, consistent with results of Hattori et al.[27], mRNA expression levels of PDGFRβ and Ang1 in rho/FGF2-tg mice were significantly increased relative to WT mice. This result is consistent with a previous study demonstrating that FGF2 can stimulate pericyte proliferation and promote pericyte recruitment by modulating PDGFRβ signaling [29]. In addition, the recruited pericytes produce Ang1, which was shown to activate Tie2 signaling and contribute to vascular maturation and stabilization [30]. Based on these reports [29, 30], we hypothesize that this signaling pathway promotes maturation and expansion of CNV in rho/FGF2-tg mice. Even on day 14 post-PC, Ang1 mRNA expression levels were significantly higher in rho/FGF2-tg mice compared to that in WT mice. This difference may be explained by the fact that Ang1 acts downstream of PDGFR activation in the signaling cascade, resulting in a relatively delayed decline in its expression and consequently leading to a significant difference in the Ang1 mRNA expression level at day 14 post-PC.

We also focused on Ang2, which functionally antagonizes Ang1 and has recently emerged as a therapeutic target for ocular neovascular diseases [31]. When VEGFA levels are high, Ang2 competes with Ang1 for binding to their receptor, Tie2, and interacts with integrin receptors to promote pericyte detachment, leading to vascular destabilization [32]. In our study, Ang2 mRNA expression levels were significantly elevated in rho/VEGF-tg mice compared to WT mice during the proliferative phase, suggesting that vascular destabilization of CNV may occur only in mice with the rho/VEGF transgene. In contrast, rho/FGF2-tg mice showed no significant change in Ang2 mRNA expression levels, suggesting that FGF2-driven angiogenesis may not be related to Ang2 regulation.

During the proliferative phase, PDGFRβ and Ang2 mRNA expression levels in rho/FGF2/VEGF-tg mice were significantly higher than those in WT mice, whereas the Ang1 mRNA expression level in

rho/FGF2/VEGF-tg mice was comparable to that observed in WT mice. These results suggest that an elevated PDGFRβ mRNA expression level reflects enhanced pericyte recruitment, which is apparent in our flat mount analysis, and ongoing vascular structural remodeling driven by FGF2. Moreover, when VEGFA is overexpressed, VEGFA-mediated suppression of PDGFRβ signaling may decrease Ang1 mRNA expression and increase Ang2 mRNA expression, thereby suppressing vascular maturation. Interestingly, the area of CNV in rho/FGF2/VEGF-tg mice was similar to that in rho/FGF2-tg mice, despite VEGFA-mediated suppression of vascular maturation. This observation suggests that, under conditions of FGF2 overexpression, an alternative angiogenic pathway, which is independent of VEGF, may contribute to CNV enlargement. Hara et al. reported an apelin–APJ pathway that increases neovascularization in a VEGF-independent manner [13]. Apelin signaling exerts proliferative effects via activation of Akt/mTOR/p70S6K, and independently of the VEGF–PKC/Raf/MEK pathway [12–14]. In our study, the apelin mRNA expression level was increased at day 7 post-PC in both rho/FGF2-tg and rho/FGF2/VEGF-tg mice, suggesting that this pathway may contribute to CNV enlargement under conditions when FGF2 is expressed.

On day 14 post-PC, PDGFRβor Apelin mRNA levels in rho/FGF2-tg and rho/FGF2/VEGF-tg mice were similar to those of WT mice, whereas on day 28 post-PC, PDGFRβor Apelin mRNA levels in rho/FGF2-tg and rho/FGF2/VEGF-tg mice were higher than those in WT mice. The mechanism for this phenomenon remains unclear and may reflect a pathway that affects PDGFRβ and apelin. This potential pathway awaits further investigation.

3. Antiangiogenic regulators: PEDF and TSP1

We also examined two endogenous antiangiogenic factors: PEDF and TSP1. PEDF binds specifically to the VEGFR2 extracellular domain to inhibit its intrinsic tyrosine kinase activity, and in turn block downstream VEGFA signaling [7].

In our study, the PEDF mRNA expression level in rho/FGF2-tg and rho/FGF2/VEGF-tg mice showed no significant change and did not correlate with CNV area. These findings suggest that PEDF mRNA expression levels do not directly reflect the extent of neovascularization and that FGF2-driven angiogenesis may not be strongly antagonized by PEDF. We initially thought, based on previous reports [35], that when VEGFA is overexpressed, PEDF expression would be upregulated as a compensatory mechanism to limit VEGF signaling. However, we observed that the PEDF mRNA expression level was, in fact, suppressed in rho/VEGF-tg mice at days 14 post-PC. One possible explanation for this result is that chronic VEGFA overproduction alters the transcriptional regulation of antiangiogenic genes that disrupts the balance between proangiogenic and antiangiogenic factors.

TSP1 can induce caspase-dependent apoptosis in endothelial cells via CD36 signaling and can also inhibit VEGF function by binding directly to VEGF or by suppressing VEGFR2 phosphorylation [33, 36]. In addition, TSP1 has been reported to bind multiple growth factors and angiogenic regulators (e.g., FGF2, TGFβ, PDGF, HGF/SF, and HIV-Tat) to inhibit their activity [34]. In our study, the TSP1 mRNA expression level in rho/FGF2-tg mice was significantly higher than that in WT mice on days 7,14 and 28 post-PC.

Based on this result, FGF2-driven CNV could be affected by antiangiogenic pressure mediated by TSP1 across all angiogenic phases. The results demonstrating that the CNV area in rho/FGF2-tg mice was large relative to that in WT mice during the proliferative phase yet was similar between rho/FGF2-tg and WT mice during the regression phase supports this possibility and reflects the potential antiangiogenic effect of TSP1. Moreover, the TSP1 mRNA expression level in rho/FGF2/VEGF-tg mice was not significantly higher than that in WT mice during the proliferative phase, suggesting that a TSP1-mediated antiangiogenic effect in rho/FGF2/VEGF-tg mice could be attenuated by VEGFA. In rho/FGF2/VEGF-tg mice without PC, the TSP1 mRNA expression level was higher than that in WT mice, which could reflect a transcriptional response by FGF2-associated retinal neovascularization, since rho/FGF2/VEGF-tg mice have retinal neovascularization but rho/FGF2-tg mice do not.

On day 28 post-PC, the TSP1 mRNA expression levels in rho/VEGF-tg and rho/FGF2/VEGF-tg mice were significantly higher than those in WT mice. This elevated TSP1 mRNA expression may cause the regression of CNV maintained by VEGFA. Notably, in rho/FGF2-tg mice, the TSP1 mRNA expression level remained higher than that in WT mice even on day 28 post-PC, when CNV lesions had nearly completely regressed. This finding suggests that TSP1 upregulation begins during the proliferative phase and persists over the long term even after CNV has regressed in FGF2-driven angiogenesis.

In this study, we evaluated Li-CNV under conditions of FGF2 and VEGFA overexpression using single and double transgenic mouse lines and an analysis that combined OCTA, flat mounts, and RT-qPCR. We showed that the CNV in rho/FGF2/VEGF-tg mice had the neovascular characteristics of VEGFA and FGF2. Moreover, we showed that vascular maturation was affected when FGF2 overexpression was added to VEGFA overexpression and that the FGF2-associated apelin pathway contributes to CNV expansion. A notable finding of our study was that the TSP1 mRNA expression level in rho/FGF2-tg mice was elevated beginning in the proliferative phase and remained high after CNV regression. This result suggests that FGF2-driven neovascularization may induce high and persistent TSP1 mRNA expression levels. Regarding the relationship between TSP1 and FGF2, Margosio et al. reported that TSP1 prevents the association of FGF2 with the matrix and mobilizes matrix-bound FGF2 in a biologically inactive form, therefore acting as a scavenger for this growth factor [37]. This earlier report supports an inhibitory role for TSP1 towards FGF2. Yamada et al. reported that the amount of retinal neovascularization spontaneously occurring in rho/FGF2/VEGF-tg mice was lower than that in single rho/VEGF-tg mice [26]. In our RT-qPCR analysis, the TSP1 mRNA expression level in rho/FGF2/VEGF-tg mice was significantly higher in animals without PC, potentially reflecting Yamada's findings that retinal neovascularization could be suppressed by a TSP1-associated negative pathway. These findings may provide a basis for the development of an anti-VEGF therapy that combines the vessel regression effects of TSP1 associated with FGF2-driven angiogenesis. However, these ideas remain highly hypothetical, and their feasibility, safety, and relevance to human diseases require comprehensive evaluation in future studies.

Limitations

This study has several limitations. First, we used mice transgenic for rho/VEGF, rho/FGF2, or a combination of VEGF and FGF2. These animals are not maintained in a natural environment, but are housed in an experimental animal setting. The mice show excessive amounts of the target proteins in certain areas. These conditions may thus affect various biological pathways in unexpected manners in vivo. For example, VEGFA overexpression in rho/VEGF-tg and rho/FGF2/VEGF-tg mice was limited to the outer retina, which may decrease its effect on Li-CNV. Although the introduction of the rho/FGF2/VEGF double transgene expanded the retinal region exposed to local VEGFA to some extent, it did not fully recapitulate the global retinal elevation of VEGF observed in some clinical cases.

Second, we did not use transmission electron microscopy (TEM), which allows cell types and ultrastructural features of the vascular wall, such as pericytes, smooth muscle cells, and intercellular junctions, to be evaluated. Although our immunostaining demonstrated that Li-CNV lesions were labeled with PDGFRα/β and α-SMA, these findings provide only indirect evidence to support vascular maturation and stability.

Third, RT-qPCR was performed on the retina-choroid complexes to ensure reliable detection of transgene expression. Consequently, in rho/VEGF-tg and rho/FGF2/VEGF-tg mice, our measurements inevitably included contributions from retinal neovascularization in addition to Li-CNV. Moreover, we did not quantify protein levels using western blotting or other methods; therefore, our mechanistic interpretations are based solely on mRNA expression levels and should be interpreted with caution. Future studies combining more localized sampling with protein quantification are required to refine these mechanistic insights.

Despite these limitations, our findings provide important insights into how VEGFA- and FGF2-driven angiogenesis differentially shapes CNV formation, maturation, and regression.

Materials and Methods

Animals

We used 6-week-old WT mice (littermates negative for both VEGFA and FGF2 transgenes), rho/VEGF-tg mice (C57BL/6J), rho/FGF2-tg mice (C57BL/6J), and rho/FGF2/VEGF-tg mice (C57BL/6J). Rho/VEGF-tg and rho/FGF2-tg mice were generously provided by Professor Peter A. Campochiaro (Wilmer Eye Institute, Johns Hopkins University, USA). Rho/FGF2/VEGF-tg mice were prepared by crossbreeding rho/VEGF-tg and rho/FGF2-tg mice.

All experiments involving animals adhered to the ARVO Statement for the Use of Animals in Ophthalmic and Vision Research and were approved by the Animal Experimentation Committee of Kansai Medical University (approval number: 25–120). Mice were housed in sterile plastic cages under a 12-h light/dark

cycle with free access to food and water ad libitum. The cages, bedding, and water were sterilized before use.

Before all procedures, anesthesia was induced by intraperitoneal injection of ketamine hydrochloride (90 mg/kg; Daiichi Sankyo, Tokyo, Japan) and xylazine (40 mg/kg; Bayer, Berlin, Germany). Pupillary dilation was achieved using a combined solution of 0.5% tropicamide and 0.5% phenylephrine (Santen Pharmaceutical Co., Osaka, Japan). Mice were euthanized by cervical dislocation before tissue collection.

Li-CNV model

Li-CNV was induced by laser PC of the left eye in each mouse. PC was performed using a 532-nm laser (GYC-2000; NIDEK Co., Aichi, Japan) connected to a slit-lamp delivery system (SL 130; Carl Zeiss, Jena, Germany). The laser parameters were set to a spot size of 100 μm, duration of 100ms, and power of 200mW. In accordance with a previous report [38], these parameters disrupted Bruch's membrane and induced CNV (Fig. 5). Three laser spots were applied in the posterior pole, avoiding major retinal vessels, and bubble formation was confirmed for each spot.

Immunohistochemistry

1. Choroidal flat mounts

To evaluate how growth factors are involved in CNV, we performed immunostaining on choroid/retinal pigment epithelium (RPE) flat mounts. At the indicated time point, mice were euthanized and their eyes were immediately enucleated. The choroid/RPE complexes were carefully dissected after fixation in 4% paraformaldehyde (PFA) in PBS for 30 min.

The following primary antibodies were used:

- CD31 (marker for endothelial cells): rat anti-mouse CD31 monoclonal antibody (MEC13.3, 1:500; BD Biosciences Pharmingen, San Diego, CA, USA), followed by Alexa Fluor Plus 488-conjugated secondary antibody (1:500).
- PDGFRα/β (marker for pericytes/mural cells): rabbit recombinant anti-human PDGFRα + PDGFRβ antibody (Y92; ab32570, 1:500; Abcam, Cambridge, MA, USA), confirmed to cross-react with mouse, followed by Alexa Fluor Plus 405-conjugated secondary antibody (1:500).
- α-SMA (marker for smooth muscle cells/RPE activation): Cy3-conjugated mouse anti-α-SMA monoclonal antibody (clone 1A4, 1:500; Sigma-Aldrich, St. Louis, MO, USA).

All antibodies were diluted in PBS containing 0.6% BlockAce (DS Pharma Biomedical, Osaka, Japan). Flat mounts were incubated with primary antibodies overnight at 4℃, thoroughly washed, and incubated with secondary antibodies overnight at 4℃. After the final wash, specimens were flattened on slides and mounted with ProLong™ Gold Antifade Mountant (Thermo Fisher Scientific, Waltham, MA, USA) before a cover slip was applied.

2. Cryosections

For cryosection analysis, the eyes were enucleated at the indicated time point, embedded in Super Cryo-embedding Medium (SCEM; Sakura Finetek Japan Co., Ltd., Tokyo, Japan), rapidly frozen on dry ice, and stored at -80℃. Cryosections (8 μm thick) were prepared using a cryostat (CM3050S; Leica Biosystems, Nussloch, Germany).

In addition to the antibodies used for flat mounts, the following primary antibodies were used for the cryosections:

- rabbit anti-human FGF2 monoclonal antibody (ab92337, 1:400; Abcam), followed by Alexa Fluor Plus 488-conjugated secondary antibody (1:500).
- rat anti-human VEGF-165 monoclonal antibody (Ultra-LEAF™ Purified anti-human VEGF-165 antibody, 1:400; BioLegend, San Diego, CA, USA), followed by Alexa Fluor Plus 594-conjugated secondary antibody (1:500).

Sections were incubated with primary antibodies overnight at 4℃, washed, and then incubated with secondary antibodies for 1 h at 37℃. After washing, sections were mounted with DAPI Fluoromount-G® (SouthernBiotech, Birmingham, AL, USA) and cover slipped.

Choroidal flat mounts and cryosections were examined using a confocal laser scanning microscope (FV4000; EVIDENT, Tokyo, Japan). Imaging parameters, including exposure time, gain, pinhole size, and laser power, were kept constant across all samples within each experiment to allow comparison of fluorescence intensity and morphology.

OCTA imaging

OCTA imaging was performed using an RS-3000 Advance system (NIDEK Co., Aichi, Japan). A 10-diopter mouse adapter was attached, and animals were positioned on a dedicated platform that stabilized them in front of the RS-3000 Advance, as described previously [39–41]. For each scan, a 750 μm × 750 μm area centered on the CNV lesion was imaged, with eight B-scans acquired at each of the 256 raster positions. The focus was adjusted to the choroidal vasculature.

To prevent corneal desiccation and lens opacification during imaging, a clear hard contact lens (OOPS Co., Kyoto, Japan) was placed on the left eye. Li-CNV lesions were imaged on days 3, 7, 14, 21, and 28 post-PC. The built-in follow-up (i.e. eye-tracking) function was used to ensure that the same lesions were imaged longitudinally in each animal.

RT-qPCR

At each time point, retina-choroid complexes were carefully dissected from the eyecup and immediately preserved in RNAlater® (Thermo Fisher Scientific) solution to prevent RNA degradation. Tissues were homogenized using a Biomasher tissue grinder (Nippi Inc., Tokyo, Japan). Total RNA was extracted using

the RNeasy Plus Mini Kit® (Qiagen, Venlo, The Netherlands) according to the manufacturer's instructions.

cDNA was synthesized from total RNA using SuperScript™ IV VILO™ Master Mix (Thermo Fisher Scientific). Real-time qPCR was performed on a Thermal Cycler Dice® Real Time System II (Takara Bio, Shiga, Japan) using TB Green® Premix Ex Taq™ II (Takara Bio) in a total reaction volume of 25 µL following the manufacturer's protocol.

Gene expression levels were calculated using the $2^{-\Delta\Delta Ct}$ method, with GAPDH as the endogenous control. Expression in untreated WT mice was used as a calibrator, and relative mRNA expression levels were displayed.
The target sequences used in this study were amplified using the following primers:

• human VEGFA; (forward) 5'- GAGCCTTGCCTTGCTGCTCTA – 3' and

(reverse) 5'- CACCAGGGTCTCGATTGGATG – 3'

• human FGF2; (forward) 5'- GGAGTGTGTGCTAACCGTTACCTG – 3' and
(reverse) 5'- TGCCACATACCAACTGGTGTATTTC – 3'

• mouse PDGFRβ; (forward) 5'- GAACGACCATGGCGATGAGA – 3' and

(reverse) 5'- GGCATCGGATAAGCCTCGAA – 3'

• mouse Ang1; (forward) 5'- CAGCCACAAAGCCTTAGTGACTTTC – 3' and
(reverse) 5'- ATCCTGTAATGTCGGCACATACCTC – 3'

• mouse Ang2; (forward) 5'- GGACTTCTAAGTGGTGGGCACAG – 3" and

(reverse) 5'- TGAACATGTAAAGCACCCAAGAG – 3'
• mouse apelin; (forward) 5'- GAGTTGCAGCATGAATCTGAGG – 3' and

(reverse) 5'- TCTGGAGGCAACATCAGTGG – 3'

• mouse PEDF; (forward) 5'- TGACATCGACCGAGAACTGAAG – 3' and

(reverse) 5'- AGCTTCACGGGTTTGCCAGTA – 3'
• mouse TSP1; (forward) 5'- GACAAGGACCTGCCACATTCA – 3' and

(reverse) 5'- CCGTCACCACAGGTCACAGA – 3'

• mouse GAPDH; (forward) 5'- TGTGTCCGTCGTGGATCTGA-3' and

(reverse) 5'- TTGCTGTTGAAGTCGCAGGAG – 3'

Quantification of CNV area

The CNV area was quantified using CD31-immunolabeled choroidal flat mounts and OCTA images. For flat mounts, CD31-positive CNV lesions on days 3, 7, 14, 21, and 28 post-PC were imaged using confocal microscopy, and lesion areas were measured using ImageJ software (National Institutes of Health, Bethesda, MD, USA).

For OCTA, the area of CNV lesions was measured on days 7 and 28 post-PC. The built-in follow-up function was used to ensure that longitudinal analysis was conducted on the same lesion in each eye. To evaluate vascular regression, the CNV area at day 7 post-PC was defined as 100% for each eye, and the residual CNV area at day 28 post-PC was expressed as a percentage comparison.

Statistical analysis

Statistical analyses were performed using JMP Student Edition software (version 18.2.1; SAS Institute Inc., Cary, NC, USA). Data distribution was assessed for normality using the Shapiro–Wilk test and for homogeneity of variance using Bartlett's test.

ΔCt values from RT-qPCR were analyzed using linear mixed-effects models, with genotype specified as a fixed effect and PCR plate as a random effect, to adjust for inter-plate differences before inter-genotype comparisons. When both normality and homogeneity of variance assumptions were satisfied, one-way analysis of variance (ANOVA) was performed. The ANOVA was followed by Tukey's honestly significant difference (HSD) test for post hoc multiple comparisons in flat mount and OCTA imaging and Dunnett's multiple comparisons test with WT at each post-PC day as the control for RT-qPCR. When either assumption was violated, the nonparametric Steel–Dwass test was used for the multiple comparisons in flat mount and OCTA imaging, and the nonparametric Steel's test was used with WT at each post-PC day as the control for RT-qPCR.

A p-value < 0.05 was considered statistically significant. In all experiments, 'n' represents the number of eyes (one eye per mouse). For flat mount quantification, 10 eyes per genotype per time point were analyzed ($n = 10$); for OCTA, 5 eyes per genotype per time point were imaged longitudinally ($n = 5$); and for RT-qPCR, retina-choroid complexes from 8 eyes per genotype per time point were used ($n = 8$).

Declarations

Acknowledgments

We extend our sincerest gratitude to all members of the Ophthalmology Research Lab at Kansai Medical University for their invaluable support and assistance throughout this study. Their collective expertise and dedication were crucial for conducting our experiments and analyzing the results. We are deeply grateful to Ms. Keiko Toyama and Professor Kanji Takahashi, former chair of the Department of Ophthalmology, for his continuous encouragement and insightful guidance throughout the course of this

work. We also extend our appreciation to the administrative staff for their valuable logistical support that facilitated this study.

Authorship contribution statement

Yuichi Yamamoto: Writing – review & editing, Writing – original draft, Visualization, Validation, Supervision, Software, Resources, Project administration, Methodology, Investigation, Formal analysis, Data curation, Conceptualization.
Haruhiko Yamada: Validation, Supervision, Project administration.
Hidetsugu Mori: Validation, Supervision.
Yuki Hattori: Methodology, Investigation.
Kaito Yokota: Methodology, Investigation.
Masatoshi Omi: Methodology, Investigation.
Megumi Kitamura: Visualization, Validation, Methodology, Formal analysis.
Masayuki Ohnaka: Supervision.
Hisanori Imai: Validation, Supervision.

Data Availability Statement

All data generated or analyzed during this study are available from the corresponding author upon reasonable request.

Funding Declaration

This research received no specific grant from any funding agency in the public, commercial, or not-for-profit sectors.

Declaration of Competing Interest

The authors declare that they have no competing financial interests or personal relationships that could have influenced the work reported in this study.

Institutional Review Board Statement

All experiments involving animals were performed in accordance with the guidelines of the ARVO Statement for the Use of Animals in Ophthalmic and Vision Research. This study was conducted in accordance with the ethical standards and guidelines for animal experimentation and was approved by the Ethics Committee of Kansai Medical University (approval number: 25-120).

Informed Consent Statement

Not applicable.

References

1. Carmeliet, P. & Jain, R. K. Molecular mechanisms and clinical applications of angiogenesis. *Nature* **473**, 298–307. https://doi.org/10.1038/nature10144 (2011).
2. Wietecha, M. S., Cerny, W. L. & DiPietro, L. A. Mechanisms of vessel regression: toward an understanding of the resolution of angiogenesis. *Curr. Top. Microbiol. Immunol.* **367**, 3–32. https://doi.org/10.1007/82_2012_287 (2013).
3. Phng, L. K. & Gerhardt, H. Angiogenesis: a team effort coordinated by Notch. *Dev. Cell.* **16**, 196–208. https://doi.org/10.1016/j.devcel.2009.01.015 (2009).
4. Alon, T. et al. Vascular endothelial growth factor acts as a survival factor for newly formed retinal vessels: implications for retinopathy of prematurity. *Nat. Med.* **1**, 1024–1028. https://doi.org/10.1038/nm1095-1024 (1995).
5. Gerber, H. P. et al. Vascular endothelial growth factor regulates endothelial cell survival through the phosphatidylinositol 3'-kinase/Akt signal transduction pathway: requirement for Flk-1/KDR activation. *J. Biol. Chem.* **273**, 30336–30343. https://doi.org/10.1074/jbc.273.46.30336 (1998).
6. Bornstein, P. Thrombospondins function as regulators of angiogenesis. *J. Cell. Commun. Signal.* **3**, 189–200 (2009).
7. Zhang, M. et al. PEDF is an endogenous inhibitor of VEGF-R2 angiogenesis signaling in endothelial cells. *Exp. Eye Res.* **213**, 108828. https://doi.org/10.1016/j.exer.2021.108828 (2021).
8. Mettu, P. S., Allingham, M. J. & Cousins, S. W. Incomplete response to anti-VEGF therapy in neovascular AMD: exploring disease mechanisms and therapeutic opportunities. *Prog Retin Eye Res.* **82**, 100906. https://doi.org/10.1016/j.preteyeres.2020.100906 (2021).
9. Broadhead, G. K. et al. How to judge failure: defining treatment resistance to anti-VEGF therapy in exudative maculopathies – a systematic scoping review. *Ophthalmol. Retina*. https://doi.org/10.1016/j.oret.2025.10.006 (2025). published online 14 Oct 2025.
10. Murakami, M. & Sakurai, T. Role of fibroblast growth factor signaling in vascular formation and maintenance: orchestrating signaling networks as an integrated system. *Wiley Interdiscip Rev. Syst. Biol. Med.* **4**, 615–629. https://doi.org/10.1002/wsbm.1190 (2012).
11. Cao, R. et al. Comparative evaluation of FGF-2-, VEGF-A-, and VEGF-C-induced angiogenesis, lymphangiogenesis, vascular fenestrations, and permeability. *Circ. Res.* 94, 664–670 (2004). https://doi.org/10.1161/01.RES.0000118600.91698.BB
12. Kim, J. et al. An endothelial apelin–FGF link mediated by miR-424 and miR-503 is disrupted in pulmonary arterial hypertension. *Nat. Med.* **19**, 74–82. https://doi.org/10.1038/nm.3040 (2013).
13. Hara, C. et al. Laser-induced choroidal neovascularization in mice attenuated by deficiency in the apelin-APJ system. *Invest. Ophthalmol. Vis. Sci.* **54**, 4321–4329. https://doi.org/10.1167/iovs.13-11611 (2013).
14. del Toro, R. et al. Identification and functional analysis of endothelial tip cell-enriched genes. *Blood* **116**, 4025–4033. https://doi.org/10.1182/blood-2010-02-270819 (2010).
15. Pereira, D. S. et al. Clinical proof of concept for anti-FGF2 therapy in exudative age-related macular degeneration (nAMD): phase 2 trials in treatment-naive and anti-VEGF pretreated patients. *Eye* **38**,

1140–1148. https://doi.org/10.1038/s41433-023-02848-7 (2024).

16. Lu, Y. et al. Safety and efficacy of multiple escalating doses of RC28-E for neovascular age-related macular degeneration: a phase 1b trial. *Ophthalmol. Ther.* **13**, 2405–2415. https://doi.org/10.1007/s40123-024-00994-z (2024).
17. Kimura, H. et al. A new model of subretinal neovascularization in the rabbit. *Invest. Ophthalmol. Vis. Sci.* **36**, 2110–2119 (1995).
18. Qiu, G. et al. A new model of experimental subretinal neovascularization in the rabbit. *Exp. Eye Res.* **83**, 141–152. https://doi.org/10.1016/j.exer.2005.11.014 (2006).
19. Wong, C. W. et al. Subchoroidal release of VEGF and bFGF produces experimental choroidal neovascularization in the rabbit. *Curr. Eye Res.* **42**, 237–243. https://doi.org/10.1080/02713683.2016.1227448 (2017).
20. Okamoto, N. et al. Transgenic mice with increased expression of vascular endothelial growth factor in the retina: a new model of intraretinal and subretinal neovascularization. *Am. J. Pathol.* 151, 281–291 PMID: 9212753. (1997).
21. Ozaki, H. et al. Basic fibroblast growth factor is neither necessary nor sufficient for the development of retinal neovascularization. *Am. J. Pathol.* **153**, 757–765. https://doi.org/10.1016/S0002-9440(10)65619-2 (1998).
22. Miller, H., Miller, B., Ishibashi, T. & Ryan, S. J. Pathogenesis of laser-induced choroidal subretinal neovascularization. *Invest. Ophthalmol. Vis. Sci.* **31**, 899–908 (1990).
23. Kano, M. R. et al. VEGF-A and FGF-2 synergistically promote neoangiogenesis through enhancement of endogenous PDGF-B–PDGFRβ signaling. *J. Cell. Sci.* **118**, 3759–3768. https://doi.org/10.1242/jcs.02483 (2005).
24. Ida, H. et al. RPE cells modulate subretinal neovascularization, but do not cause regression in mice with sustained expression of VEGF. *Invest. Ophthalmol. Vis. Sci.* **44**, 5430–5437. https://doi.org/10.1167/iovs.03-0609 (2003).
25. Tobe, T. et al. Evolution of neovascularization in mice with overexpression of vascular endothelial growth factor in photoreceptors. *Invest. Ophthalmol. Vis. Sci.* **39**, 180–188 (1998).
26. Yamada, H. et al. Cell injury unmasks a latent proangiogenic phenotype in mice with increased expression of FGF2 in the retina. *J. Cell. Physiol.* **185**, 135–142. https://doi.org/10.1002/1097-4652(200010)185:1%3C135::AID-JCP13%3E3.0.CO;2-Y (2000).
27. Hattori, Y. et al. The effect of fibroblast growth factor 2 on neovascular vessels depends on the stage of angiogenesis. *Heliyon* 10, e39843 (2024). https://doi.org/10.1016/j.heliyon.2024.e39843
28. Greenberg, J. I. et al. A role for VEGF as a negative regulator of pericyte function and vessel maturation. *Nature* **456**, 809–813. https://doi.org/10.1038/nature07424 (2008).
29. Hosaka, K. et al. Dual roles of endothelial FGF-2–FGFR1–PDGF-BB and perivascular FGF-2–FGFR2–PDGFRβ signaling pathways in tumor vascular remodeling. *Cell. Discov*. **4**, 3. https://doi.org/10.1038/s41421-017-0002-1 (2018).

30. Liu, Z. L. et al. Angiogenic signaling pathways and anti-angiogenic therapy for cancer. *Signal. Transduct. Target. Ther.* **8**, 198. https://doi.org/10.1038/s41392-023-01460-1 (2023).
31. Shirley, M. Faricimab: first approval. *Drugs* **82**, 825–830. https://doi.org/10.1007/s40265-022-01713-3 (2022).
32. Thurston, G. & Daly, C. The complex role of angiopoietin-2 in the angiopoietin–Tie signaling pathway. *Cold Spring Harb Perspect. Med.* **2**, a006550. https://doi.org/10.1101/cshperspect.a006650 (2012).
33. Lawler, P. R. & Lawler, J. Molecular basis for the regulation of angiogenesis by thrombospondin-1 and – 2. *Cold Spring Harb Perspect. Med.* **2**, a006627. https://doi.org/10.1101/cshperspect.a006627 (2012).
34. Margosio, B. et al. Fibroblast growth factor-2 binding to the thrombospondin-1 type III repeats, a novel antiangiogenic domain. *Int. J. Biochem. Cell. Biol.* **40**, 700–709 (2008).
35. Ohno-Matsui, K. et al. Vascular endothelial growth factor upregulates pigment epithelium-derived factor expression via VEGFR-1 in human retinal pigment epithelial cells. *Biochem. Biophys. Res. Commun.* 303, 962–967 PMID: 12670505. (2003).
36. Suzuma, K. et al. Expression of thrombospondin-1 in ischemia-induced retinal neovascularization. *Am. J. Pathol.* **154**, 343–354. https://doi.org/10.1016/S0002-9440(10)65281-9 (1999).
37. Margosio, B. et al. Thrombospondin 1 as a scavenger for matrix-associated fibroblast growth factor 2. *Blood* **102**, 4399–4406. https://doi.org/10.1182/blood-2003-03-0893 (2003).
38. Nakagawa, K. et al. Comparison between optical coherence tomography angiography and immunolabeling for evaluation of laser-induced choroidal neovascularization. *PLoS One*. **13**, e0201958. https://doi.org/10.1371/journal.pone.0201958 (2018).
39. Park, J. R. et al. Imaging laser-induced choroidal neovascularization in the rodent retina using optical coherence tomography angiography. *Invest. Ophthalmol. Vis. Sci.* **57**, OCT331–OCT340. https://doi.org/10.1167/iovs.15-18946 (2016).
40. Shah, R. S. et al. Visible-light optical coherence tomography angiography for monitoring laser-induced choroidal neovascularization in mice. *Invest. Ophthalmol. Vis. Sci.* **57**, OCT86–OCT95. https://doi.org/10.1167/iovs.15-18891 (2016).
41. Alnawaiseh, M. et al. OCT angiography in the mouse: a novel evaluation method for vascular pathologies of the mouse retina. *Exp. Eye Res.* **145**, 417–423. https://doi.org/10.1016/j.exer.2016.02.012 (2016).

Figures

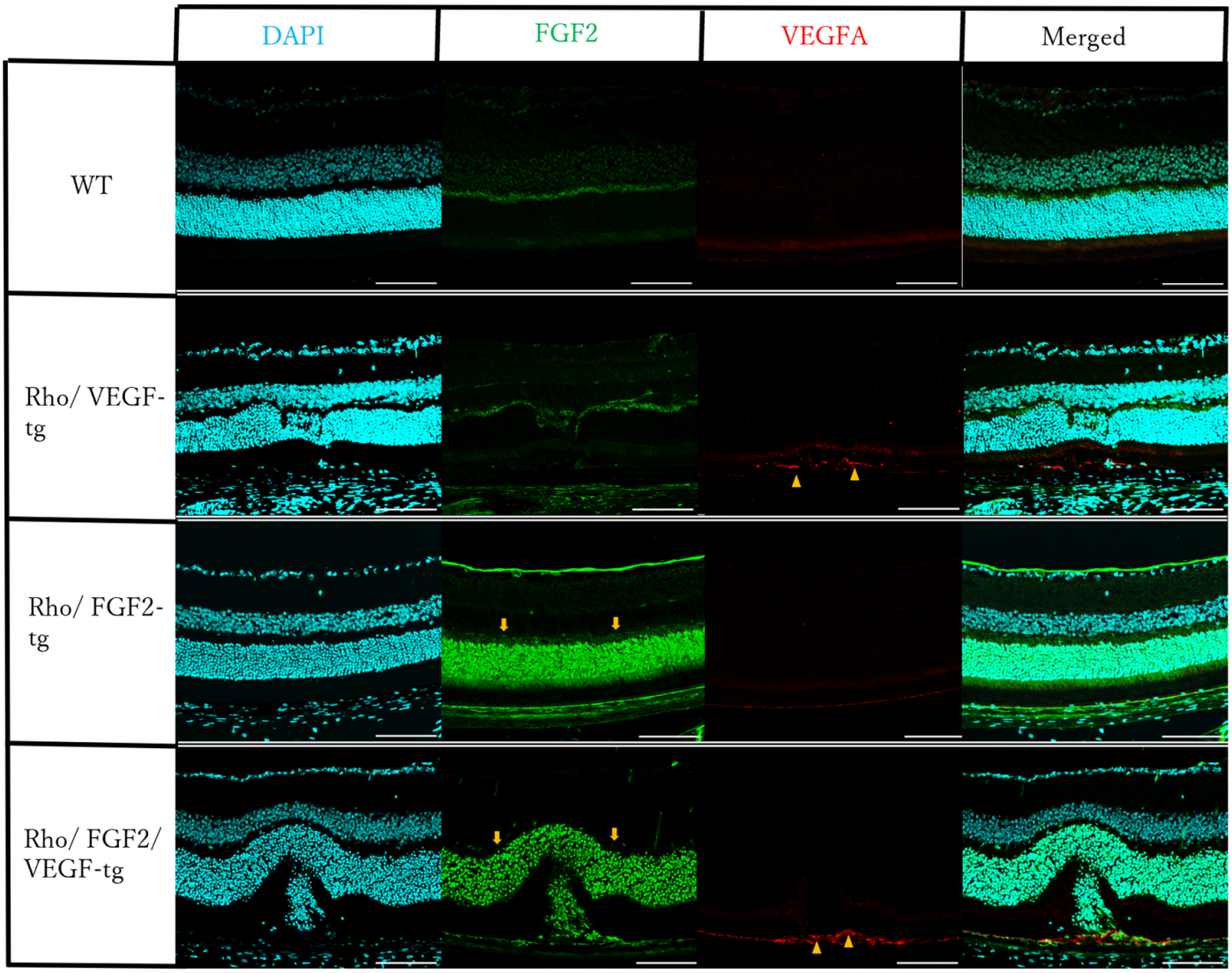


Figure 1

Immunofluorescence of retinal cryosections from WT, rho/VEGF-tg, rho/FGF2-tg, and rho/FGF2/VEGF-tg mice. 20× objective. Scale bar = 100 μm.

Light blue: DAPI staining; Green: immunofluorescence staining with an anti-human FGF2 antibody; Red: immunofluorescence staining with an anti-human VEGFA antibody. The panel on the far right shows the merged image.

Arrows and arrowheads indicate positive signals for human FGF2 and human VEGFA, respectively.

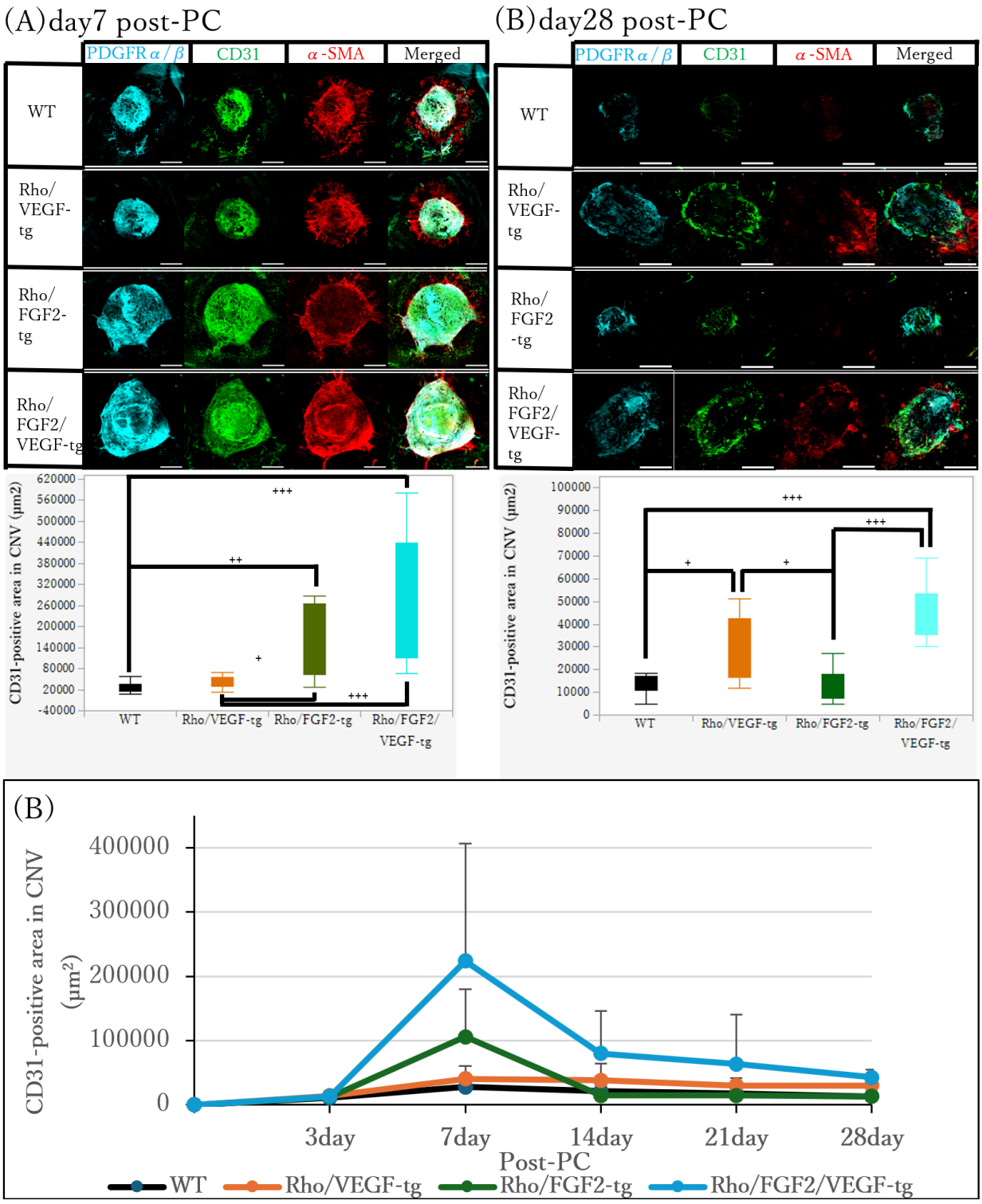


Figure 2

Quantification of Li-CNV and choroidal flat mount immunostaining in WT, rho/VEGF-tg, rho/FGF2-tg, and rho/FGF2/VEGF-tg mice.

Light blue: PDGFRα/β; Green: CD31; Red: α-SMA; Rightmost panel: merged image. 20× objective. Scale bar = 200 μm.

(A): Choroidal flat mount images (upper) and quantification of the CD31-positive Li-CNV area (lower) on day 7 post-PC. (B): Choroidal flat mount images (upper) and quantification results of the CD31-positive Li-CNV area (lower) on day 28 post-PC. (C): Time-dependent changes in the CD31-positive area in CNV after PC.

Data show mean ± SD. $^{+}p < 0.05$, $^{++}p < 0.01$, $^{+++}p < 0.005$, Steel–Dwass test, n = 10.

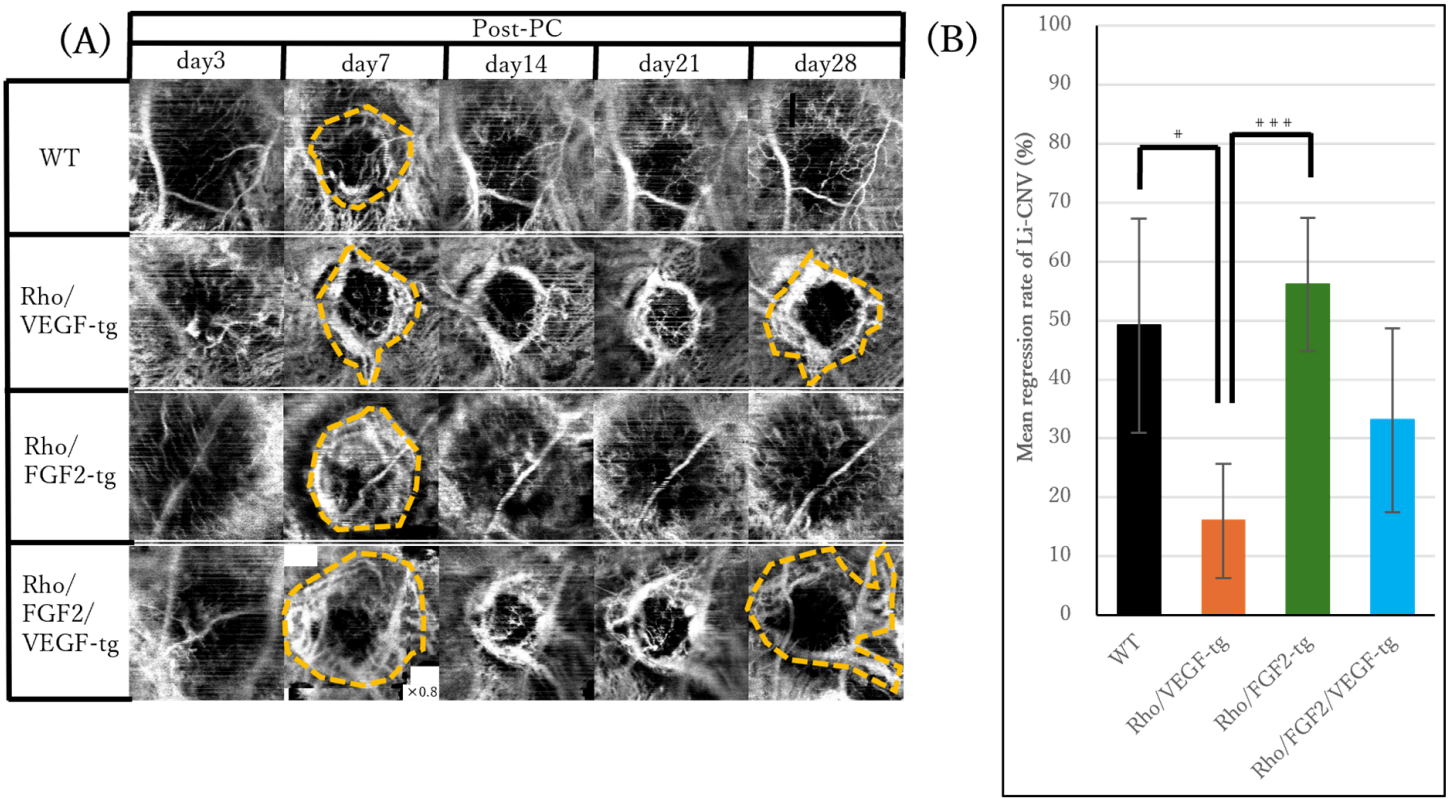


Figure 3

OCTA images and CNV regression rates in WT, rho/VEGF-tg, rho/FGF2-tg, and rho/FGF2/VEGF-tg mice.

(A) OCTA images at days 3, 7, 14, 21 and 28 post-PC for each genotype. Yellow dashed lines indicate Li-CNV area. (B) Comparison of Li-CNV regression rates, which were calculated using the formula (CNV area on day7-CNV area on day28)/ CNV area on day7 x100.

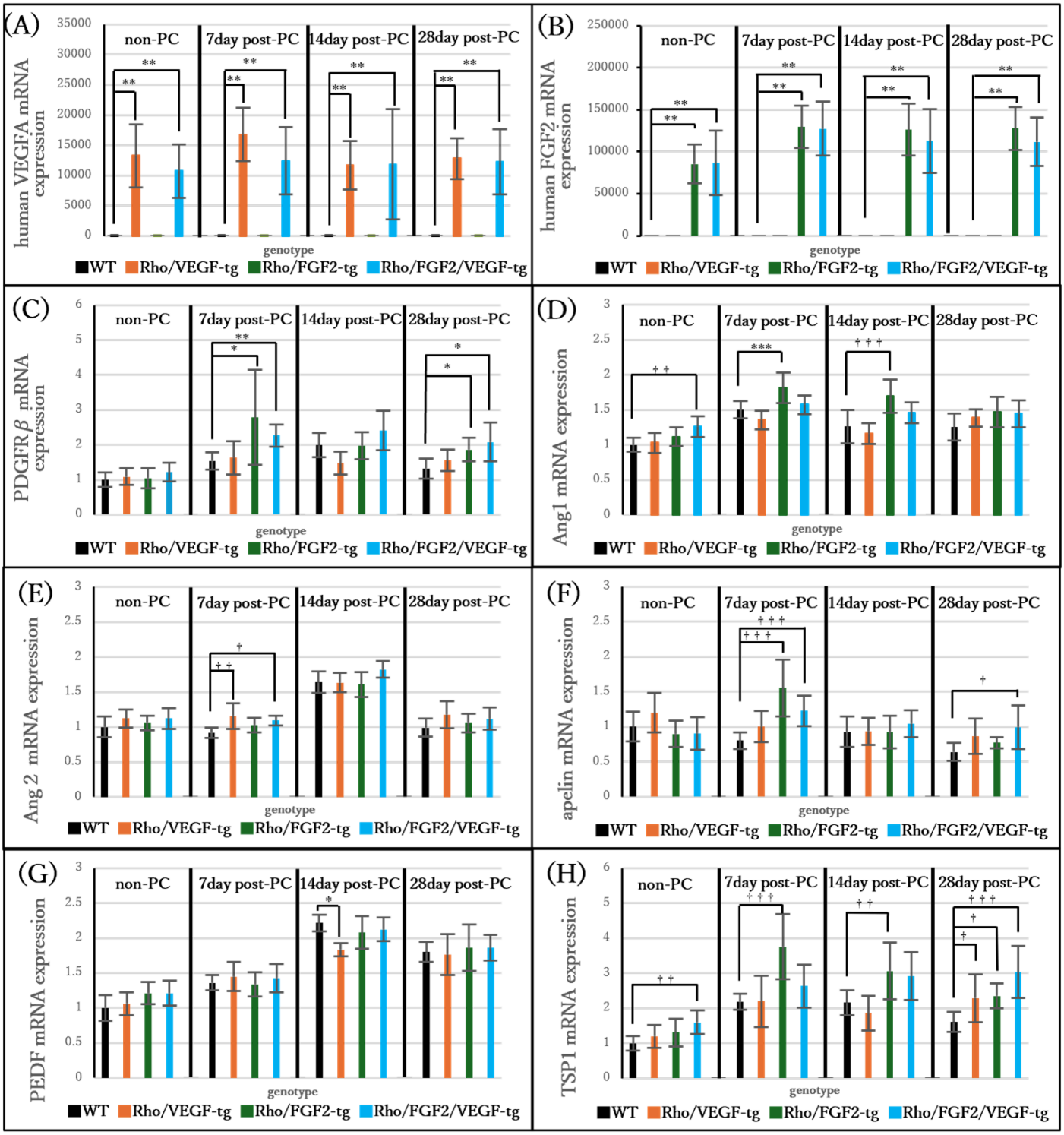


Figure 4

Real-time qPCR analysis of WT, rho/VEGF-tg, rho/FGF2-tg, and rho/FGF2/VEGF-tg mice

Gene expression levels were calculated using the 2−ΔΔCt method, with GAPDH as the endogenous control and untreated WT mice as the calibrator. Data are presented as relative mRNA expression levels. Statistical analyses between the different types of transgenic mice data are not shown in these figures.

mRNA expression levels are shown for (A) VEGFA; (B) FGF2; (C) PDGFRβ; (D) Ang1; (E) Ang2; (F) Apelin (G) PEDF; and (H) TSP1.

Data shown are the mean ± SD. *,†p < 0.05, **,††p < 0.01, ***,†††p < 0.005, *Steel's test with WT at each post-PC day as the control, †Dunnett's multiple comparisons test with WT at each post-PC day as the control, n = 8.

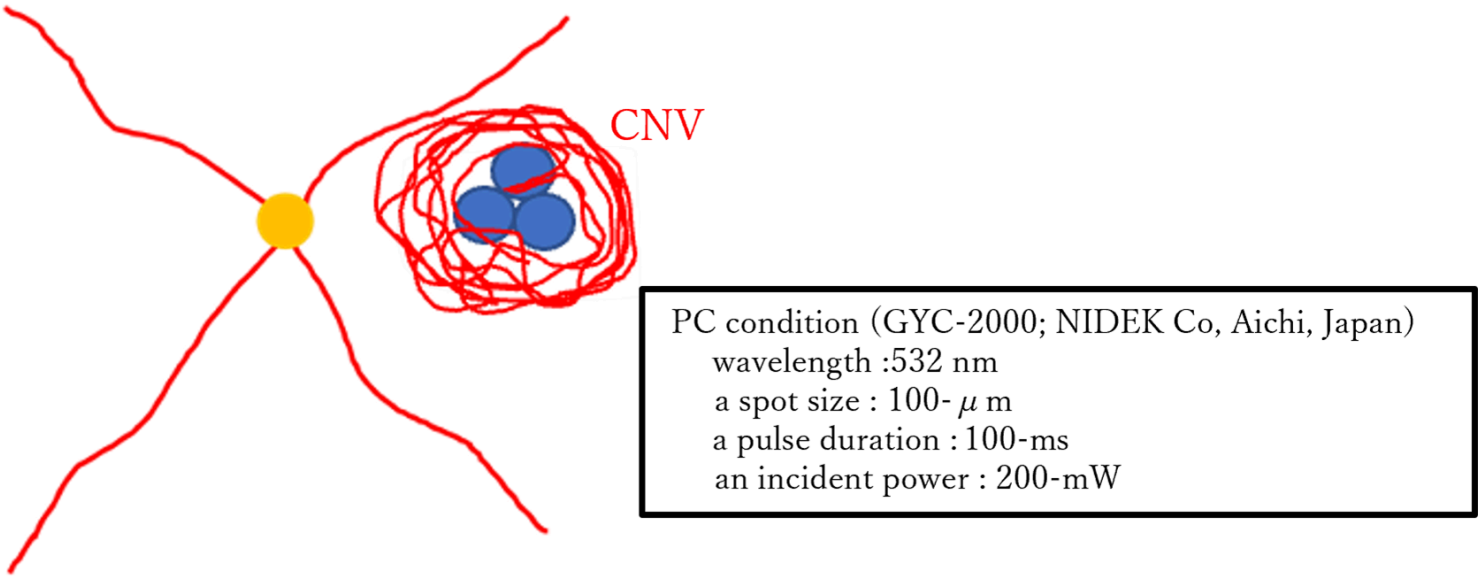


Figure 5

Schematic diagram of the Li-CNV model

Photocoagulation (PC) was performed by applying three laser burns adjacent to the retina, as shown (blue circles). Bubble formation was confirmed after each laser application. After PC, Li-CNV gradually developed around the PC spots (red circular nests). The laser parameters used for PC are indicated in the figure.